· Article · Advances in Polar Science
doi:10.12429/j.advps.2025.0014 March 2026 Vol. 37 No. 1: 56-69

On the possibility of the subglacial lake formation on islands of Franz Josef Land archipelago, Russian Arctic

Sergey POPOV[1,2*], Yulia KAZBANOVA[2], Sofia SHERSTENNIKOVA[2] & QIAO Gang[3,4]

[1] Department of the Geology and Mineral Resources of the Antarctic, Gramberg All-Russian Scientific Research Institute for Geology and Mineral Resources of the World Ocean (VNIIOkeangeologia), Saint Petersburg 190121, Russia;
[2] Institute of Earth Sciences, Saint Petersburg State University, Saint Petersburg 199178, Russia;
[3] College of Surveying and Geo-Informatics, Tongji University, Shanghai 200092, China;
[4] Center for Spatial Information Science and Sustainable Development Applications, Tongji University, Shanghai 200092, China

Received 3 June 2025; accepted 7 January 2026; published online 30 March 2026

Abstract This study investigates the potential formation of subglacial lakes beneath the glaciers of the Franz Josef Land archipelago, Russian Arctic, under current and future climatic conditions. Using a one-dimensional heat and mass transfer model, the research evaluates the influence of geothermal heat flow, ice thickness, and surface temperature on basal melting. The model incorporates enthalpy formulation and boundary conditions derived from field data, including temperature profiles and geothermal measurements. Results indicate that subglacial lakes could form under ice masses exceeding 300 m thickness, driven by geothermal heating, though current basal temperatures remain below the melting point. Simulations under the IPCC SSP1-2.6 scenario suggest a gradual warming trend, highlighting the long-term thermal inertia of Arctic glaciers. The study underscores the need for enhanced observational data to validate models and improve predictions of glacial dynamics in response to climate change.

Keywords **Arctic, Franz Josef Land, subglacial lakes, mathematical modelling**

Citation: Popov S, Kazbanova Y, Sherstennikova S, et al. On the possibility of the subglacial lake formation on islands of Franz Josef Land archipelago, Russian Arctic. Adv Polar Sci, 2026, 37(1): 56-69, doi: 10.12429/j.advps.2025.0014

1 Introduction

Climate changes are indicated by slightest elements of environment. For instance, subglacial lakes are unique hydro-glacial objects which differ from common or glacial lakes by being located under glacier and being isolated from atmosphere for thousands and even millions of years (Livingstone et al., 2022). These objects are of special interest due to their uniqueness. In particular, exploring them, especially with remote methods, leads to broad prospects of receiving new data about what Earth was like in the past when these very lakes were not isolated. These objects are widely common in polar regions, generally in the area of massive glacier shield, Greenland and Antarctic, although they are some lakes on Canadian archipelago and in Alps (Livingstone et al., 2022). This is explained by their genesis. Results of math modeling done at the dawn of exploring Antarctica have shown that average-planetary geothermal heat flow (GHF) is enough to boost bedrock melting under quite thick glaciers which was demonstrated earlier research by Robin (1955) and Zotikov (1963).

Thus, melted water fills negative bedrock landforms

* Corresponding author. ORCID: 0000-0002-1830-8658. E-mail: s.popov@vniio.ru, s.popov@spbu.ru

and forms subglacial lakes. Since the most massive glaciers are located in Antarctica and Greenland, then absolute majority of subglacial lakes are found in these very areas. The biggest and the most well-known is Lake Vostok, located near Russian Antarctic station Vostok (Kapitsa et al., 1996; Popov et al., 2024a; Ridley et al., 1993). Antarctic lakes are varied in morphology and ecology: there are salty, fresh or containing biota. Arctic subglacial lakes are generally located in Greenland. They are significantly smaller and rarer, generally found close to glacier edge due to slope glacial processes. Their detection is performed using radio-echo sounding (RES) and high-precision satellite altimetry (Popov et al., 2024a; Schroeder et al., 2020). There are also some small lakes in Iceland, as the geothermal flow from subglacial volcanos compensates for the limited thickness of glacier. Russian Arctic is an uncommon region for the study of subglacial lakes. It is a large region including both Arctic and subarctic climates, so it is necessary to examine selection of climate factors for each archipelago. Island fragmentation is also a peculiar feature preventing glacial cover from growing thick. Nevertheless, there are glaciers hundreds of meters thick. At the same time, the temperature there is much higher. This circumstance is capable of compensating, to some extent, for the ice thickness required for lake formation. Besides, small lakes are more sensitive to climate change, which can either hinder or promote subglacial lake formation (Livingstone et al., 2022). Thus, there is no recorded evidence of the existing of any significant subglacial lakes in Russian Arctic under current climate environment.

However, there is available tools for climate environment reconstruction in past and future such as math modeling. The aim of the recent research is to reveal physical possibility and conditions for the formation of subglacial lakes under Russian Arctic glaciers nowadays and in the context of standard climate warming scenario. The models used in the work are a well-recongnized way of exploring the cryolithozone and broadly applied for exploring subglacial lakes in the non-direct way (Fürst et al., 2011; Greve and Blatter, 2009; Pattyn, 2003, 2010), but are mostly commonly applied to Antarctica. Due to the factors mentioned above, modeling is less frequently applied to Arctic glaciers which has led to disproportion in collected data. Present research pursuits to fill up this gap and clarify possibility of formation of subglacial lakes in Russian Arctic. The results obtained allow to track how specific environmental elements react to climate fluctuation.

2 Study region

2.1 Climate

Franz Josef Land archipelago, washed by the Barents Sea to the west and the Kara Sea to the east, is the northernmost in the Russian Arctic. Its dimension is about 250 km from north to south and 400 km from west to east. The archipelago's climate is defined by its geographical location and Gulf Stream washing it to the west. Due to its high-latitude location, the Sun does not rise high above the horizon. Arctic climatic front which is forming wind rose is situated to the south from archipelago. Besides, it is far from the continent.

As a result of mentioned factors, an Arctic polar climate is forming. Meteorological observations have been conducted by Ernst Krenkel Observatory on Hayes Island since 1957 in this region (Figure 1). According to these records, the radiation balance for archipelago is negative. The mean annual air temperature does not exceed −12 ℃; it can drop below –40 ℃ in winter and does not go above +2 ℃ in summer. Precipitation ranges from 200–300 mm per year by the shore and 500−550 mm per year in the glacial accumulation zone (Krenke and Voronina, 1964). Air humidity averages 85% in winter and 92% in summer, although it might go below 50% in winter on Rudolf Island due to the Föhn effect. Average wind velocity is 7–9 $m \cdot s^{-1}$ with a maximum of about 40 $m \cdot s^{-1}$. Katabatic winds have been recorded on the ice capes (Krenke and Voronina, 1964). Basic meteorological features based on observations for 1966–2022 are presented in Figure 2.

The meteorological data used in this study, obtained from the Ernst Krenkel Observatory (Hayes Island) via the All-Russian Research Institute of Hydrometeorological Information-World Data Center (RIHMI-WDC), underwent a multi-tiered quality control procedure. This process encompassed internal verification by Roshydromet, involving automated checks for physical plausibility and adherence to climatic norms, inter-station control, and mandatory manual validation. It further included automated filtering of anomalous outliers and integrity checks at the RIHMI-WDC platform level, supplemented by an independent author-led analysis. The latter involved assessing the extent and distribution of data gaps, along with visual and statistical scrutiny of time series to identify anomalies. Short-term gaps were reconstructed using a persistence method (replacement with the last valid observation), whereas prolonged gaps were excluded from the dataset. The selection of the Ernst Krenkel Observatory dataset was justified by its superior data representativeness, a condition of paramount importance for ensuring the validity of the numerical experiments.

Climate fluctuations are closely related to archipelago glaciations both in chronicle times and the Pleistocene and Holocene. The lowest temperatures for Franz Josef Land as well as for the entire Arctic were reconstructed at the end of Pleistocene during the Last Glacial Maximum (LGM) when the archipelago was covered with the Eurasian glacier. According to isotope analysis in ice wedges of the polar regions of Russia, temperatures during LGM (18–21 ka) were from 8.5 ℃ to 13.5 ℃ lower than today (Surkova and Vasil'chuk, 2022). Research conducted in the West Siberia, where glaciation was similar to that of the Arctic at that time, shows that average winter temperature anomaly was

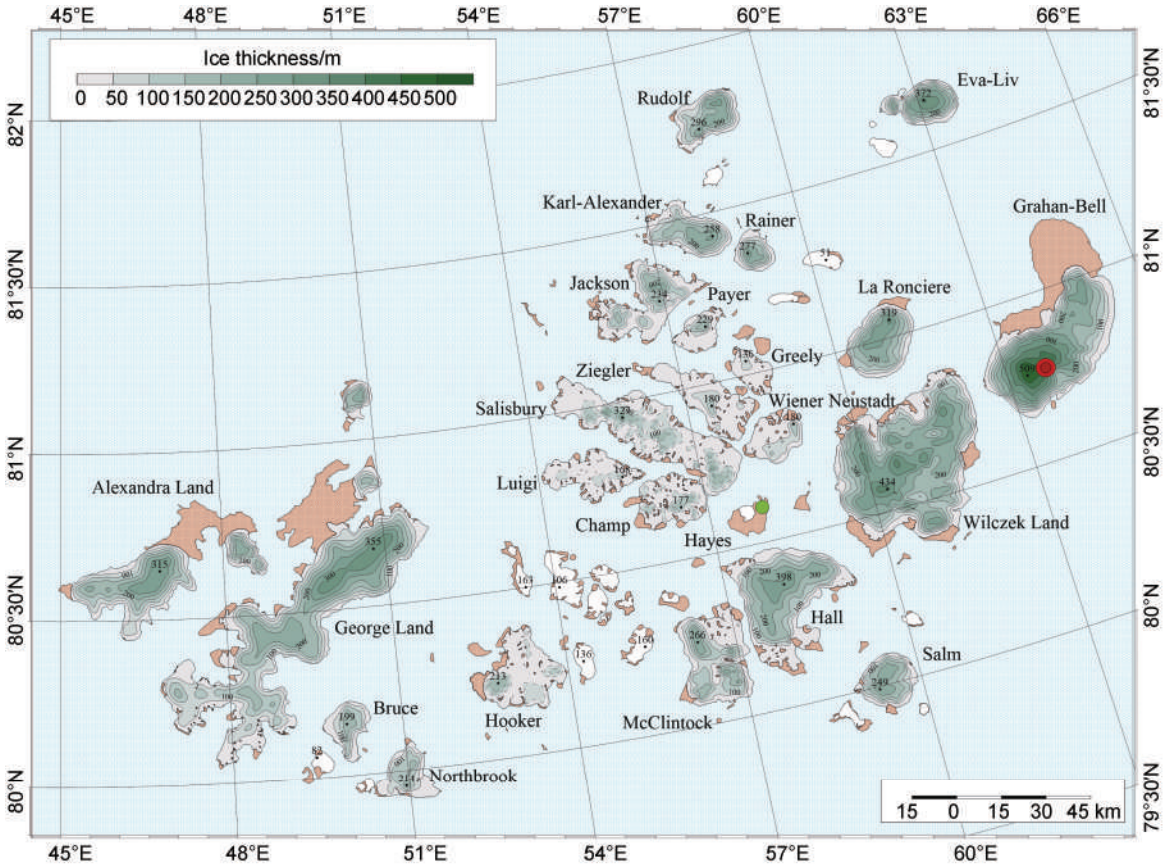

Figure 1 Ice thickness of the study area. Ice thickness contours, contour interval is 50 m. Drilling site is depicted by the red dot. The meteorological station is depicted by the green dot.

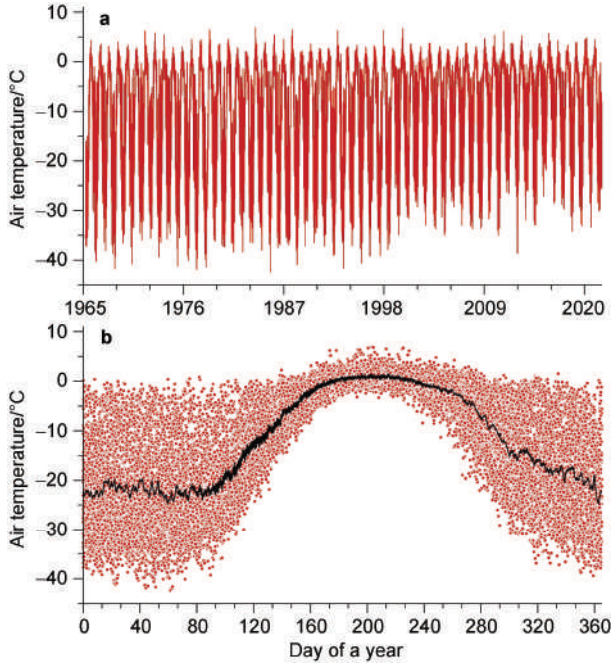

Figure 2 Air temperature for period 1966–2022 (**a**) and air temperature day-to-day averaging (**b**). The black line is depicted by averaged data and red points are measured data. The time series starts on 1 January, 1966.

between −7.9 ℃ and −7.0 ℃ compared to nowadays (Vasil'chuk and Surkova, 2020). Besides, there were periods of regional cooling and warming in chronical times. Evidence of Little Ice Age (LIA) around 16th–18th centuries was reconstructed from ice cores from Hooker, Leigh-Smith, Northbrook and Hall islands (Lubinski et al., 1999). According to them and also some cores from Svalbard, the annual temperature was 1–2 ℃ lower than the modern one (Fransworth et al., 2020). There are also Svalbard cores with evidence of warm periods after LIA around AD 1750 that contain sediments like pits that commonly mark warm climate (Virkkunen et al., 2007).

2.2 Ice thickness and glaciation

A complex of oceanographic and climate factors (slight effect of warm Gulf Stream and high-latitude location) results in the fact that islands with high thickness of glaciers are situated in this very region. Generally, glaciation is characterized by ice sheet in the middle part of archipelago and with outlet glaciers carrying out the outflow on the periphery.

According to modern knowledge, ice cover extends over 85.1% of archipelago land area (13,735 km^2). Outlet glaciers areas are no more than 2%–3% of the total glacier territory (the biggest one is Znamenityi on Wilczek Land

which has 30 km in length and 382 km^2 in area). The most extensive glacier complexes cover George Land (2,152 km^2), Wilczek Land (1,884 km^2) and Graham Bell Island (1,215 km^2). Glacier thickness is moderate, with the average of about 180 m and a maximum of 509 m, recorded on the Graham Bell Island. The glaciation is asymmetrical with a strong predominance in the eastern part. There are three morphological types of glaciers: plateau glaciers, valley glaciers and small glaciers. Plateau glaciers are generally confined to flat surfaces of igneous intrusions on the western and central islands and also to sand strata on the eastern islands. Their forms are either ice capes (Čiurlionis, Yuri and Bezymyanni capes) or ice sheets (Lunnyi, Brusilov and Tumannyi sheets). Valley glaciers are the thickest on the archipelago. They are confined to linearly elongated depressions and forms glacier cirques (glaciers of Nepristupnykh rock on Salisbury Island) and also merges in glacier tongues forming some type of glaciers on benches (Helen glacier on Hooker Island). Small glaciers might be niche, cirques, hanging and in form of flat-top combs. The mentioned types can combine to form complex glacier systems: cover, cover-reticular, reticular-foothill and plateau glacier system (Groswald et al., 1973).

Ice thickness on islands reaches 500 m (Figure 1) according to airborne radio-echo sounding data collected by the Polar Marine Geosurvey Expedition in 1993, 1998 and 1999 (Khlyupin et al., 2002; Leonov and Popov, 1997). Eva-Liv and Freden islands are fully covered with ice, although Eva-Liv's glacier is an ice cap thicker than 300 m and Freden's glacier is a shallow iceberg with the similar thickness. Graham Bell Island is about 80% covered by a glacier. This glacier is an ice sheet with a thickness of up to 500 m, with outlet glaciers in the southern and eastern parts. Salm Island, the southernmost island of the archipelago, is also an ice cap with a thickness of up to 300 m, with outlet glaciers on the periphery. The glaciation of one of the largest islands, Wilczek Land, has a similar characteristic. In its eastern part there is an outlet glacier, which covers more than a third of the island's territory, carrying out the outflow of the ice sheet, which occupies the entire central and western parts. In the northeast, there is an ice cap with a thickness of 30–50 m located near the mountain exits. It is quite possible that part of the tongue of the eastern outlet glacier is afloat. The entire central part of La Roncierre Island is covered with an ice cap with a thickness of 300–400 m, on the periphery of which there are numerous outlet glaciers. There is an ice cap with a thickness of more than 300 m in the north and east of Rudolf Island. The extended ice-free uplift in the south of the island prevents ice from flowing into the sea. About 80% of the territory of Karl-Alexander Island is covered with an ice cap, the main flow of which is carried out by the outlet glacier located in the eastern part. The thickness of the glacier on the Hall and McClinton islands is approximately the same, and is 200–300 m. The entire central part of Jackson Island is covered with an ice cap. Its flow is obstructed by the mountain outcrops bordering the island. Ziegler Island is almost completely free of ice (or the thickness of its ice cover does not exceed a 10 m). Minor glaciers with a thickness of about 100 m are located in the south and southwest. Similar glacier thicknesses are observed on Salisbury Island. The data obtained indicate that the tongues of some outlet glaciers are afloat, but their size, most likely, covers no more than 5%–7% of the island's territory. The methodology of work and data processing has been published in the works of Leonov and Popov (1997) and Khlyupin et al. (2002).

There are two types of ice formation temperature regimes on Franz Josef Land: wet-cold in the cold snow-firn zone and continental in the ice zone and ablation zone. The first type is typical of 30% of the glacial cover of the archipelago (mainly in the eastern and central parts), and the remaining 70% of glaciers belong to the zone of the continental temperature regime. The average ice temperature at a depth of 15–20 m is −9 ℃; it is −10 ℃ for glaciers with direct ice formation and from −4 ℃ to −2.5 ℃ for glaciers with firn formation. The active layer, within which annual temperature fluctuations occur, does not exceed 20 cm. Glaciers are underlain by frozen rocks with a sufficiently low temperature: according to the results of measurements in 1959, the rocks under the dome of Čiurlionis had a temperature of −11.8 ℃ (Groswald et al., 1973).

Unfortunately, the Russian Arctic region has not yet been studied well enough. This also applies to the glaciers of the archipelago. The authors found only one temperature profile. In 1997, a large 315-m ice core were drilled on the top of Windy Dome cape (Kupol Vyetrenyi), Graham Bell Island (Figure 1). Researchers obtained data about ice characteristics including density, pore filling, ion structure and four physically different types of ice (bubbly, meltwater, firn and icy firn). Unfortunately, this core covers only the first 315 m out of 509 m (Henderson, 2002). The temperature profile is shown in Figure 3.

Density of clear (meltwater) ice remained constant (920 kg·m^{-3}) for the whole core, while the rest of them fluctuated with the depth. According to laboratory analysis, the density of firn and icy firn in the upper parts of the cores is similar to ice density and is about 920 kg·m^{-3} (Henderson, 2002). It is quite possible that this density peculiarity is caused by dynamic infiltration processes during the intervening past times.

2.3 Bedrock topography and GHF

The concept of the subglacial topography is formed on the basis of the mentioned data of the thickness of the glacial cover. Analysis of the data obtained shows that the relief of the rocky base (both subglacial and ice-free) is represented by plains and plateaus no higher than 450 m, as well as low-lying plains with absolute heights of less than 150 m with indistinct coastal outlines. For this study, the geological structure of the archipelago is an important

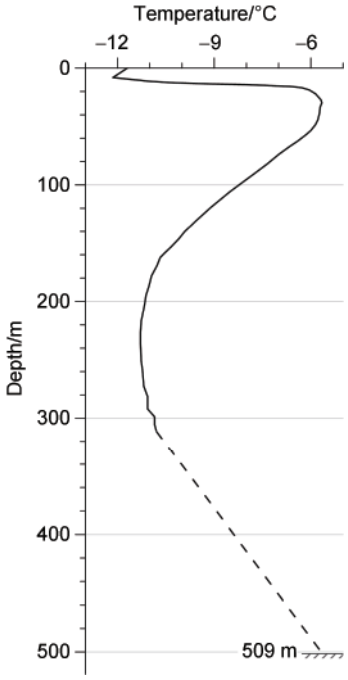

Figure 3 Temperature distribution in the central part of Windy Dome (Henderson, 2002). Data were collected in 1997.

aspect, since it is directly related to the permeability of the subglacial surface and the magnitude of the GHF. Geological and airborne geophysical data indicate that the glacier bed is mainly underlain by crystalline rocks (Gramberg et al., 1985; Karyakin and Kashkarov, 2011). This means that when bottom melting occurs, meltwater will accumulate without seeping into the ground, thus forming subglacial reservoirs in negative forms of subglacial relief.

The neotectonic movements within the archipelago inherit the trend of Jurassic–Cretaceous spreading and rifting, driven by the destruction of the mantle plume beneath the lithosphere of the Arctic region, in particular, the Barents Sea Plate (Shipilov et al., 2018). The magnitude of the geothermal flow obtained during deep drilling varies from 30 to 97 $mW \cdot m^{-2}$ (Khutorskoy et al., 2013). High heat fluxes indicate that most wells are confined to the active fault zones of the region and that there is a tendency for heat flux to increase in the northeast and northwest directions.

3 Model description

3.1 Formulation of the model

The estimates of the possibility of bottom melting and the formation of subglacial reservoirs presented below are based on modeling the process of heat and mass transfer in glaciers, implemented by numerically solving the heat equation. Of course, to improve the quality of modeling, it is important to take into account the spreading of the glacier, and the associated release of additional heat. This approach has been implemented in a number of models published in papers by Fürst et al. (2011), Greve and Blatter (2009), Pattyn (2003, 2010), and many others. However, one must keep in mind that the more complex the model, the more factors it takes into account, and, as a result, the more different data it requires. In this sense, to obtain reliable results, a reasonable compromise is needed between the models and the quality of the data they use. The conflict between data and models is well illustrated in Vinogradov (1988). As can be seen from the above review, providing glaciers in the Russian sector of the Arctic with glacio-geophysical data can hardly be considered good. Therefore, there are reasonable doubts about the real improvement of our estimates by using complex models. On the other hand, there are numerous examples where one-dimensional modeling produces acceptable results. These include the basal melting models by Robin (1955) and Zotikov (1963). Recent one-dimensional modeling conducted for the central part of Lake Dålk demonstrated a convergence between modeled and measured values of approximately 0.5% (Sukhanova et al., 2023). However, it should be noted that in areas with significant horizontal ice flow velocities, the performance of one-dimensional modeling would deteriorate.

Due to the mentioned facts, we consider a one-dimensional model of heat and mass transfer. In general, this approach has proven itself well in similar works by the authors (Boronina et al., 2024; Popov et al., 2023, 2024b; Sukhanova et al., 2023). For calculations, we consider a glacier section located within a certain speculative negative relief shape to ensure the formation of a lake water layer (Ω_W) in the presence of bottom melting. As shown above, the geological structure of the islands of the Franz Josef Land archipelago is quite diverse, but the stone base of the bedrock (Ω_G), on which the glacier rests, is composed mostly of waterproof rocks. We also consider a classical glacier consisting of atmospheric ice (Ω_I) with a thickness of T_I and a snow-firn stratum (Ω_S) composing its near-surface part with a thickness of T_S. Over time, snow cover can either appear during the precipitation of solid precipitation, or disappear during the summer snowmelt. Thermophysical processes on the surface of a glacier are determined by its heat exchange with the atmosphere, and on the bottom by the geothermal heat flow (Λ_G). The last one is determined by the geological structure of the Earth's crust in the research area. In case of bottom melting, it is possible to form a layer of water (Ω_W) with a thickness T_W. Hereafter, the indexes I, S, W, and G denote belonging to ice, snow, water, and rock.

Figure 4 shows an illustration of the above reasoning. The vertical axis is directed upwards, and is aligned with the stationary (on the scale of geological time) subglacial surface. The horizontal axis is the time from the start of the simulation. The figure shows a one-year section of it, typical for seasonal processes.

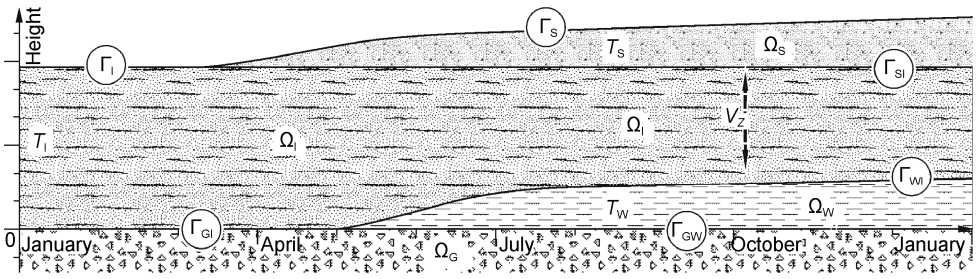

Figure 4 Illustration of the mathematical model (change in the top of the geological section with time).

Ω_I is a glacier; Ω_W is a water layer; Ω_S is snow cover (if exists); Ω_G is bedrock; Γ_P is the lower boundary of the computational domain; Γ_S and Γ_I are the upper boundaries of the computational domain; Γ_{SI} is boundary between snow and ice; Γ_{GI} is the boundary between ice and bedrock; Γ_{GW} is boundary between melted water and bedrock; Γ_{WI} is boundary between ice and water. T_I, T_S and T_W are thickness of ice, snow and water, respectively; V_Z is the vertical movement rate.

3.2 Governing and state equations

A one-dimensional approximation is considered in which the thickness of a glacier changes only due to the processes of freezing/melting at its bottom, accumulation/ablation on its surface. Thus, any processes related to the movement of mass or energy in the horizontal direction are not taken into account. The main difficulty of the model lies in the possible presence of phase boundaries, the position of which changes over time. There may be several of them, and they can either form or disappear, depending on the conditions. These processes are described when solving the so-called Stefan problem (Samarskii and Moiseyenko, 1965). Without going into theoretical issues, which are sufficiently explored, in particular, in the works by Samarskii and Vabishchevich (2003, 2009), we note that for subsequent numerical implementation, it is advisable to present it in the enthalpy form:

$$\left[\rho c + q_F \delta(\theta - \theta_F)\right]\frac{\partial \theta}{\partial t} = \frac{\partial}{\partial z}\left(\lambda \frac{\partial \theta}{\partial z}\right) + V_Z \frac{\partial \theta}{\partial z} + \Phi,$$
$$z \in \{\Omega_W,\ \Omega_I,\ \Omega_S\}, \quad (1)$$

where θ is the temperature of the medium, z is the current planned coordinate, t is the time, q_F is the latent heat of melting (q_F= 333 kJ·kg^{-1}); ρ, c, and λ are the density of the environment, as well as its specific heat and thermal conductivity; V_Z is the vertical velocity of the media. The International System of Units (SI) requires the temperature should be in Kelvin, but Celsius is a more practical system. For this reason, here and below Celsius is used and K_0=273.15 K is the melting temperature at an atmospheric pressure of 1,010 hPa (Paterson, 1994). Then in the calculations, it was assumed that the values of ρ, c, and λ for ice and water are constant: ρ_I=920 kg·m^{-3}, c_I=2,060 J·kg^{-1}·℃$^{-1}$, λ_I=2.22 W·m^{-1}·℃$^{-1}$, ρ_W=1,000 kg·m^{-3}, c_W=4,212 J·kg^{-1}·℃$^{-1}$, λ_W=0.569 W·m^{-1}·℃$^{-1}$. Snow is a multicomponent environment, most generally consisting of particles of ice, moisture, and air. In the framework of this model, we consider the relations given in the works (Osokin et al., 1999; Sosnovsky, 2006):

$$\lambda_S = 9.165\times10^{-2} - 3.814\times10^{-4}\rho_S + 2.905\times10^{-6}\rho_S^2 \quad (2)$$

In this publication c_S=2,100 J·kg^{-1}·℃$^{-1}$.

Snow density ρ_S is an important parameter as it is incorporated into Equations (1) and (2). Several models of snow compaction exist, notably those by Motovilov and Zhidkov (1986), Kominami et al. (1998), and Marshall et al. (1999). In the present study, the model by Gelfan and Moreido (2014) was employed, according to Equation (3).

$$\rho_S(t) = \rho_S(0)\frac{T_S}{(T_S - v_S t)}, \quad (3)$$

where $\rho_S(t)$ is the snow density after a certain time t, $\rho_S(0)$ is its initial density, T_S is the snow thickness, and v_S is the compaction velocity, which at a depth h_S is given by Equation (4).

$$v_S(h_S) = 2.78\times10^{-7}\overline{\rho}_{S+}h_S^2\exp(0.08\theta_S - 0.021\overline{\rho}_{S+}), \quad (4)$$

where $\overline{\rho}_{S+}$ is the average density of the overlying layers, and θ_S is their temperature. The initial density, i.e., the density of freshly fallen snow ρ_{S0} is determined in accordance with Hedstrom and Pomeroy (1998) as Equation (5):

$$\rho_{S0} = \rho_{SMIN} + 51.3\exp(\theta_A/\theta_{SMIN}), \quad (5)$$

where ρ_{SMIN}=67.9 kt·m^{-3}, θ_{SMIN}=2.6 ℃, and θ_A is an air temperature.

The second term on the right-hand side Equation (1) is related to the physical movement of the environment. In this case, it is associated with the processes of bottom melting or degradation of a subglacial lake. However, it is missing at the time of the start of the modeling (and it is not known whether it will be formed). In addition, even with the presence of bottom melting, the vertical movement rates (V_Z) are very low, and even for the Antarctic glacier they amount to the first units of millimeters per year (Popov, 2022). However, the deformation of the glacier, caused by the need for the formed cavities to flow as a result of bottom melting, occurs slowly. According to Glen's law, this velocity depends on the thickness of the glacier (Glen, 1953). In particular, the authors' calculations show that a subglacial channel with an area of 1 m^2 and a glacier thickness of 600 m will completely drain in about 2 a (Boronina et al., 2024). Thus, due to the low deformation rates, this term is

neglected in the calculations. The last term in the right-hand side Equation (1) is related to the release of heat during friction of moving layers relative to each other. Since the physical movement of the glacier is neglected in the framework of subsequent calculations, the contribution of this term to the process of heat and mass transfer is also not taken into account. The temperature of the phase transition (θ_F) depends on the pressure (P) (Paterson, 1994).

$$\theta_F = -PC_F \tag{6}$$

According to the same source, the Clausius-Clapeyron C_F gradient for ice is C_F=74.3 ℃·GPa.

3.3 Boundary and initial conditions

The formulation of the boundary value problem Equation (1) requires the presence of initial and boundary conditions. It is known that for large time intervals of modeling, the former plays a noticeably smaller role than the latter. After some time, the distribution of the modeled parameter (in our case, temperature) is completely controlled by the boundary conditions. It is quite obvious that it is best to use field measurement data as initial conditions. However, this is not always possible, in particular, as in our case. The choice of initial conditions is discussed below.

Let's turn to the boundary conditions. As mentioned above, the value of the geothermal flow Λ_G is set at the lower boundary of Γ_L, which is quite justified from a geological point of view. It depends on the structure of the Earth's crust and is determined by the temperature gradient in wells, or by modeling based on geophysical data, for example, as done for Antarctica (Martos et al., 2017). As indicated in the above review, for the Franz Josef Land archipelago, it averages about 60 mW·m^{-2}. At the upper boundary of Γ_U, it is advisable to set a condition for heat exchange with the atmosphere. Both conditions can be written as follows:

$$\lambda(z)\left.\frac{\partial\theta}{\partial z}\right|_{\Gamma_L} = \Lambda_G, \quad \lambda(z)\left.\frac{\partial\theta}{\partial z}\right|_{\Gamma_U} = \alpha_E(\theta_0 - \theta_E), \tag{7}$$

where α_E and θ_E are effective parameters and θ_0 is temperature of ice surface. It should be noted that the description of the heat exchange process is generally very difficult and includes many empirical relationships and coefficients. However, when applied to the surface of snow and ice, there are expressions involving α_E and θ_E that accurately describe this process (Sosnovsky, 1984, 2006):

$$\begin{aligned}\alpha_E &= \alpha\left(1+1.95\times10^{-2}a\right)+0.205\left[\left(\theta_A-K_0\right)/100\right]^3\\ \theta_E &= \left\{\alpha\left[\left(\theta_A-K_0\right)-1.95\times10^{-2}\left(b-p_A\omega_A\right)\right]+19.9\left[\left(\theta_A-K_0\right)/100\right]^4+\Lambda_S\right\}/\alpha_E\end{aligned}, \tag{8}$$

where α is heat transfer of surface coefficient, θ_A is air temperature, p_A and ω_A are elasticity of saturated water vapor at temperature θ_A and relative air humidity accordingly. Coefficient a and b describe a linear approximation $p_A(\theta)$, $p_A(\theta)=a\theta+b$. Heat transfer α for snow, can be estimated by the ratio α=3.4+2.2v_W, where v_W is wind speed (Osokin and Sosnovsky, 2015). Using Equation (8) to model the gradual freezing of Lake Dålk (Princess Elizabeth Land, East Antarctica), it was shown that the relative accuracy in determining the thickness of frozen ice between the field measurements and the model values for the estimated times of 1 a and 3 a was about 0.5% (Sukhanova et al., 2023).

In the second equation of the relations (8) the value of the total solar radiation flux is included Λ_S. Following Sivkov's view (1968), we are counting three factors: correction for sun height and optical transparency of atmosphere (ζ_H), as well as cloudiness (ζ_C) and surface albedo (A).

$$\Lambda_S = \Lambda_{SOL}\zeta_H\zeta_C(1-A)\sin h \tag{9}$$

The sine of the sun height above the horizon ($\sin h$) might be calculated by the astronomical relations using the computer code provided by Paul Schlyter (http://stjarnhimlen.se/comp/tutorial.html). This algorithm provides a calculation error of less than one arc minute, which is quite sufficient for our calculations. According to NASA data, Solar constant (Λ_{SOL}) is 1.362 kW·m^{-2}. The parameter $\aleph$ is called number of optical air masses, which is a relative measure of the length of the Solar rays in the atmosphere (Sivkov, 1968).

$$\aleph = 2\left(\sin^2 h + \sin h + 0.003147\right)^{-1/2} \tag{10}$$

Then height correction by Kastrov (1956).

$$\zeta_H = 1.04 - 0.16\sqrt{\aleph\left(0.949\zeta_P + 0.051\right)}, \tag{11}$$

where ζ_P is relation of pressures of atmospheric air at the height H and at sea level which is equal to $\ln\zeta_P = -\mu gHR^{-1}\left(\theta_A - K_0\right)^{-1}$, where R is the universal gas constant (R=8.31 J·mol^{-1}·℃$^{-1}$) and μ is the molar mass of air (μ=0.029 kg·mol^{-1}).

The cloudiness correction (ζ_C) was calculated as Sivkov (1968).

$$\zeta_C = 1 - 0.38(1+\psi) \tag{12}$$

where ψ is cloudiness.

For the surface albedo (A) in Equation (9), there are a number of relationships, in particular Eckel and Thams (1939) as well as Prohaska and Thams (1940), but we used a more modern representation published in Dickinson et al. (1986):

$$A = A_{SNEW}\left(1 - 0.2\frac{t_{SD}}{1+t_{SD}}\right), \tag{13}$$

where A_{SNEW} is albedo of freshly fallen snow (A_{SNEW}=0.9), and t_{SD} is the age (*i.e.* the time elapsed since the last snowfall) of the top layer in days. If the top layer of snow is melted, then the albedo is between 0.4 and 0.55.

All parameters included in Equations (9)–(12) might be either calculated or obtained from the meteorological data.

The initial conditions are determined by the available temperature data from the wells, or, in their absence, by general glaciological concepts, and in general can be specified by some temperature distribution by depth $\theta_{\mathrm{INI}}(z)$:

$$\theta(z)\big|_{t=0} = \theta_{\mathrm{INI}}(z) \tag{14}$$

3.4 Numerical solution

The boundary value problem presented in enthalpy form Equation (1) with boundary conditions in Equation (7) and initial conditions in Equation (14) was solved by the finite difference method. For this purpose, Equation (1), taking into account the assumptions made, was presented in the form of an implicit four-point finite difference scheme.

$$\frac{\theta_j^{n+1}-\theta_j^n}{\Delta t} = \frac{2}{\left(\Delta z_{j-1}+\Delta z_j\right)}\left(a_{\Delta j+1/2}\frac{\theta_{j+1}^{n+1}-\theta_j^{n+1}}{\Delta z_j} - a_{\Delta j-1/2}\frac{\theta_j^{n+1}-\theta_{j-1}^{n+1}}{\Delta z_{j-1}}\right),$$
$$z\in\{\Omega_{\mathrm{W}},\ \Omega_{\mathrm{I}},\ \Omega_{\mathrm{S}}\}, \tag{15}$$

where $\Delta z_j = z_{j+1} - z_j$, index j and n correspond to the node number of the planned coordinates and time and a_Δ is smoothed thermal conductivity coefficient, $a_\Delta \equiv \lambda_\Delta/(\rho_\Delta \cdot c_\Delta)$, and ρ_Δ, c_Δ, and λ_Δ is according smoothed environmental parameters.

$$\rho_\Delta = \begin{cases} \rho_{\mathrm{W}}, \theta-\theta_{\mathrm{F}} > \Delta\theta_{\mathrm{F}},\ z\in\Omega_{\mathrm{W}} \\ \rho_{\mathrm{I}}, \theta-\theta_{\mathrm{F}} < \Delta\theta_{\mathrm{F}},\ z\in\Omega_{\mathrm{I}} \\ \rho_{\mathrm{S}}, \theta-\theta_{\mathrm{F}} < \Delta\theta_{\mathrm{F}},\ z\in\Omega_{\mathrm{S}} \\ \rho_{\mathrm{I}} + K(\theta)\dfrac{\rho_{\mathrm{W}}-\rho_{\mathrm{I}}}{2}, \left|\theta-\theta_{\mathrm{F}}\right| \leqslant \Delta\theta_{\mathrm{F}} \end{cases}, \tag{16}$$

$$\lambda_\Delta = \begin{cases} \lambda_{\mathrm{W}}, \theta-\theta_{\mathrm{F}} > \Delta\theta_{\mathrm{F}},\ z\in\Omega_{\mathrm{W}} \\ \lambda_{\mathrm{I}}, \theta-\theta_{\mathrm{F}} < \Delta\theta_{\mathrm{F}},\ z\in\Omega_{\mathrm{I}} \\ \lambda_{\mathrm{S}}, \theta-\theta_{\mathrm{F}} < \Delta\theta_{\mathrm{F}},\ z\in\Omega_{\mathrm{S}} \\ \lambda_{\mathrm{I}} + K(\theta)\dfrac{\lambda_{\mathrm{W}}-\lambda_{\mathrm{I}}}{2}, \left|\theta-\theta_{\mathrm{F}}\right| \leqslant \Delta\theta_{\mathrm{F}} \end{cases}, \tag{17}$$

$$c_\Delta = \begin{cases} c_{\mathrm{W}}, \theta-\theta_{\mathrm{F}} > \Delta\theta_{\mathrm{F}},\ z\in\Omega_{\mathrm{W}} \\ c_{\mathrm{I}}, \theta-\theta_{\mathrm{F}} < \Delta\theta_{\mathrm{F}},\ z\in\Omega_{\mathrm{I}} \\ c_{\mathrm{S}}, \theta-\theta_{\mathrm{F}} < \Delta\theta_{\mathrm{F}},\ z\in\Omega_{\mathrm{S}} \\ c_{\mathrm{I}} + K(\theta)\dfrac{c_{\mathrm{W}}-c_{\mathrm{I}}}{2} + q_{\mathrm{F}}\rho_{\mathrm{W}}\delta_\Delta(\theta), \left|\theta-\theta_{\mathrm{F}}\right| \leqslant \Delta\theta_{\mathrm{F}} \end{cases} \tag{18}$$

The difference scheme assumes the presence of an irregular grid, which significantly increases the accuracy of the calculations. The method of its formation is described by Popov (2023). The width of the smoothing temperature range $\Delta\theta$ is defined as $\Delta\theta = \left|\theta_{j+1}^n - \theta_{j-1}^n\right|$ with a condition of $\left(\theta_{j+1}^n - \theta_{\mathrm{F}}\right)\left(\theta_{j-1}^n - \theta_{\mathrm{F}}\right) < 0$.

The smoothing method c_Δ differs from ρ_Δ and λ_Δ near the phase transition temperature. This is due to the fact that the enthalpy formulation of the problem implies the formation of fictitious heat sources at such boundaries. They replenish the energy balance associated with the phase transition, taking into account the specific heat of melting of ice, which is an analogue of the classical Stefan boundary condition (Samarskii and Moiseyenko, 1965; Samarskii and Vabishchevich, 2003). This point sources are described by discrete analogue of Dirac δ-function δ_Δ.

$$\delta_\Delta(\theta) \equiv \frac{1}{\Delta\theta_{\mathrm{F}}\sqrt{2}}\exp\left[-\frac{\left(\theta-\theta_{\mathrm{F}}\right)^2}{2\Delta\theta_{\mathrm{F}}{}^2}\right] \tag{19}$$

Following Vasilyev et al. (2021), coefficient ρ, c, and λ near phase transition temperature is smoothed with function of the Gaussian normal distribution function, then

$$K(\theta) \equiv 1 + \mathrm{erf}\left(\frac{\theta-\theta_{\mathrm{F}}}{\Delta\theta_{\mathrm{F}}\sqrt{2}}\right), \tag{20}$$

$$\mathrm{erf}(x) \equiv \frac{2}{\sqrt{\pi}}\int_0^x \exp\left(-t^2\right)\mathrm{d}t \tag{21}$$

With this approach, the phase transition occurs in a certain, very small, temperature range, which, in general, is quite physical. The values of ρ, c, and λ was assumed according to the previous description.

It must also be kept in mind when calculating that density difference between ice and water leads to volume fluctuation due to phase transformations and an additional phase boundary offset by $\Delta\xi$. In particular, when freezing amount of water (ξ), $\Delta\xi = \xi(\rho_{\mathrm{W}} - \rho_{\mathrm{I}})/\rho_{\mathrm{I}}$; when melting the same amount of ice, the value $\Delta\xi$ will be the same but with a minus sigh.

4 Numerical experiments

4.1 Experiment 1 influence of start conditions

As was stated above, with reference to the experience of the authors (Popov et al., 2023, 2024b), the boundary conditions have a much greater impact on the modeling results than the initial ones. But this is true only if long-term calculations are carried out. In short periods of time, the influence of the initial conditions is very significant. This will be shown using this numerical experiment. It is logical to exclude as much as possible the influence of those external factors that lead to a change in the environment. These are precipitation events. On the one hand, they change the thickness of the glacier, and on the other hand, due to firming or complete melting of snow, they lead to a change in the thermophysical parameters of its surface part. Thus, for the entire time interval of the simulation, we set cyclically changing meteorological parameters (ambient air temperature, humidity, cloudiness, wind strength, etc.) with a period of 1 a. To do this, we average them day by day over the observation period of 1966–2022. Air temperatures are shown in Figure 2. The upper part of the geological section for subsequent modeling is represented by 200 m glacial ice lying on a waterproof rocky ground. Thus, when bottom melting occurs, meltwater accumulates, followed by the formation of a subglacial reservoir. We assume that

there is no subglacial reservoir at the initial moment of time. According to the Equation (6), at an ice density of 920 kg·m^{-3}, its melting temperature at a depth of 200 m is 0.13 ℃. The initial temperature distribution set in the glacier column to be constant, equal to −0.5 ℃. The magnitude of GHF is considered constant, equal to 60 mW·m^{-2}. The total modeling period will be 300 a. Of course, the same climatic conditions cannot be maintained for 300 a. In addition, the configuration of glacier, including its thickness, will change due to spreading. But this hypothetical example is intended to show the effect of initial conditions on the modeling process.

The results are shown in Figure 5. The first one shows the change in the temperature distribution in the bottom of the glacier over time, and the second one shows the temperature profiles along the depth at a given time.

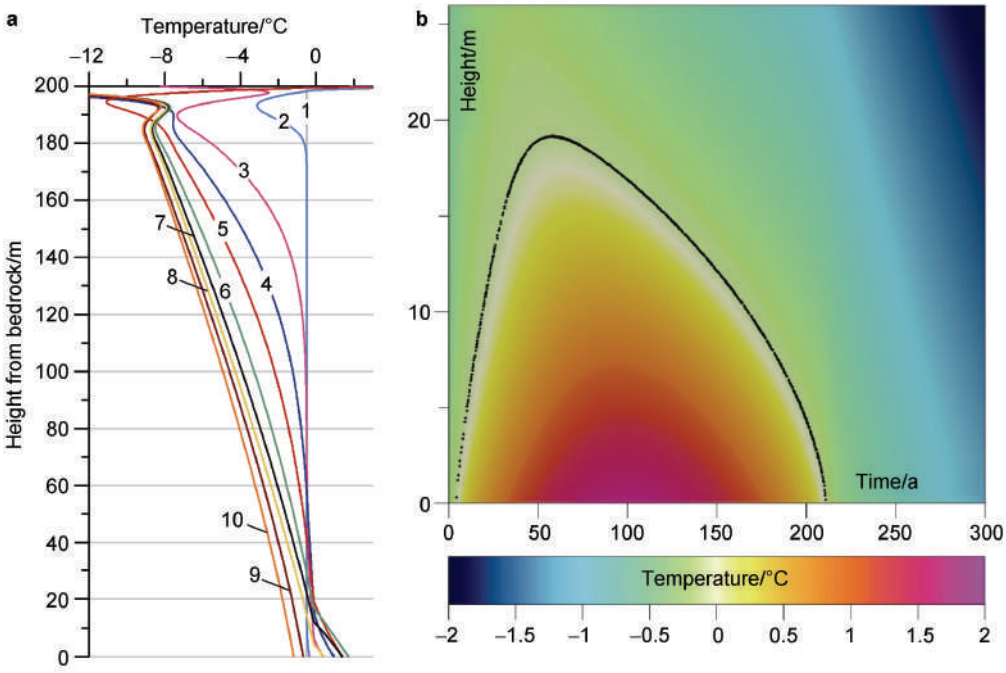

Figure 5 Results of numerical experiment 1. **a**, temperature sections; **b**, distribution. 1, initial distribution. Temperature sections in profile 2 is 0.69 a; 3 is 27.77 a; 4 is 32.10 a.; 5 is 56.44 a; 6 is 100.01 a; 7 is 150.15 a; 8 is 200.02 a; 9 is 250.03 a, and 10 is 300 a. Phases are depicted by black in section **b**.

The initial temperature distribution is constant over depth 1 (Figure 5a). This means that there is no GHF from the glacier to the rocky ground at the initial moment of time. However, from the rocky ground to the glacier, it is equal to 60 mW·m^{-2}. To comply with the law of conservation of energy, starting from the next time step, the temperature gradient in the bottom of the glacier must comply with the Neumann boundary condition (9), which is 0.027 ℃·m^{-1}. This, in turn, leads to an increase in temperature at the lower boundary of the computational domain, and, as a result, a gradual bending of the temperature profiles 2, 3, 4 and 5 (Figure 5a). An increase in temperature will occur until the system reaches an equilibrium state. In turn, the average temperature at the depth of the attenuation of seasonal fluctuations is much lower than this value, so the temperature profile also gradually bends in the upper part of profiles 2, 3, 4 and 5 (Figure 5a).

At the time of 3.84 a after the beginning of the modeling, the bottom temperature reached the temperature of the phase transition. After that, a subglacial lake gradually began to form. Its depth reached its greatest value of 19.14 m at 56.44 a after the start of modeling (Figure 5b). This is clearly visible in the temperature profile 5 (Figure 5a). Due to the almost four-fold differences in the thermal conductivity coefficients of ice and water, a visible kink in the temperature profile is observed at the phase boundary. At this point in time, the calculated temperature at the bottom of the lake was 1.4 ℃, while the bottom temperature gradient corresponds to the energy balance at the phase boundary. However, the temperature profile has not yet reached equilibrium, and it continued to bend, with the temperature gradient at the phase boundary increasing (profile 6, Figure 5a). This led to the fact that the heat flow from the glacier became greater than from the lake, i.e. its cooling and degradation followed. The lake completely froze after about 211 a from the beginning of the simulation (Figure 5b). The temperature at the ice-rock contact continued to drop further (profiles 7, 8, 9 and 10, Figure 5a). The temperature gradient in the ice column leveled off about 150 a after the start of the modeling (profile 7, Figure 5a).

Thus, we have shown that an unsuccessful choice of initial conditions initially led to incorrect calculation results.

However, as time passed and the relaxation processes ended, the contribution of the initial conditions to the calculations noticeably weakened, giving way to boundary conditions. This means that the correctness of the calculations began to increase.

4.2 Experiment 2 Windy Dome, averaged current climatic conditions

For the second numerical experiment, we take the central part of the Windy Dome, and as initial conditions, we use the temperature distribution shown in Figure 3, i.e., we supplement it with a temperature trend corresponding to a GHF of 60 mW·m^{-2}. Then the temperature at the bottom of the glacier will reach −5.42 ℃. The boundary conditions are the same as in the previous case. We set the modeling time interval from 1997 (the moment of data acquisition at the site) to 2100. The simulation results are shown in Figure 6.

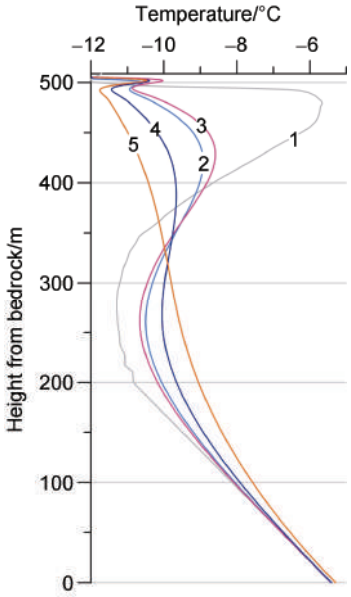

Figure 6 Temperature sections for the numerical experiment 2. 1, initial distribution. Temperature in profiles 2, 3, 4 and 5 is in 2000, 2021, 2050 and 2100, respectively.

The initial temperature distribution 1 (Figure 6) demonstrates a gradual decrease from about the depth of attenuation of seasonal fluctuations (altitude 490 m) to about 250 m. This is followed by its growth. The decrease in temperature, as mentioned above, is associated with the general cooling of the glacier during the epoch of maximum glaciation. After 3 a (in 2000), the temperature on the glacier bed practically did not change, but it began to level out slightly along the section, naturally tending to a steady state of 2. Twenty-four years after the initial moment (2021), the leveling of the abnormally low temperature area began to reduce the gradient of the lower part of the temperature profile 3. This led to the fact that, in order to maintain the gradient corresponding to the heat flow of 60 mW·m^{-2}, the temperature at the bottom of the glacier began to gradually and systematically increase from that moment on. This is clearly shown on the temperature profiles after 53 and 103 a (curves 4 and 5), which corresponds to the beginning of 2050 and 2100, respectively. At the end of the model calculations, the temperature on the bed sooner or later will reach −5.23 ℃.

Certainly, according to the estimates presented, both at the present moment and by 2100, the subglacial lake has not formed at the estimated point, but the steady temperature trend leaves no doubt that this will happen later. The temperature change on the glacier bed is shown in Figure 7.

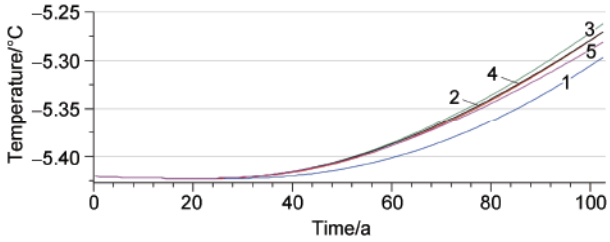

Figure 7 Temperature on the bottom of the glacier. Curve 1 for the current climatic conditions; curve 2 for the climatic conditions IPCC SSP1-2.6 and constant ice thickness; curve 3 for the climatic conditions IPCC SSP1-2.6 and ice thickness degradation of 1 m·a^{-1}; curve 4 for the climatic conditions IPCC SSP1-2.6 and ice thickness degradation of 2 m·a^{-1}; and curve 5 for the climatic conditions IPCC SSP1-2.6 and ice thickness degradation of 3 m·a^{-1}.

4.3 Experiment 3 Windy Dome, climatic conditions IPCC SSP1-2.6

Thus, the current numerical experiment implements the SSP1-2.6 scenario for the previous Windy Dome point. The selection of the SSP1-2.6 scenario for this study was driven by a specific rationale. The primary goal was not to assess the full range of possible climate outcomes but to demonstrate the fundamental response of the glacier's thermal regime to global warming under the most optimistic mitigation pathway. This approach allows us to establish a conservative baseline and explore the lower bound of expected changes. The significant shifts identified even under this favorable scenario are particularly revealing. Should more severe pathways such as SSP2-4.5 or SSP3-7.0 materialize, the consequences for glacier thermodynamics would be qualitatively similar but quantitatively more pronounced and likely catastrophic. Thus, this investigation serves as a critical foundation for subsequent analyses of more pessimistic climate trajectories. The initial conditions are the same. The IPCC scenario is launched starting in 2022, when the range of meteorological data available to the authors ends. Up to this point, real data is used. This scenario was chosen because it is the most optimistic in determining the trajectory of development of socio-economic systems and energy policy within the

framework of modern climate models. It involves the active introduction of technologies aimed at reducing greenhouse gas emissions, the transition to renewable energy sources, improving energy efficiency and sustainable land use. This leads to limiting global warming to much below 2 ℃ relative to pre-industrial levels, in line with the goals of the Paris Agreement. As a result, by 2100, the SSP1-2.6 scenario is characterized by an increase in the concentration of greenhouse gases in the atmosphere, leading to warming of 2 ℃.

The nature of the temperature distribution change in the glacier thickness is completely similar to the previous one, and the expected bottom melting has also not begun (Figure 7, line 2). By the time of 2100, the temperature on the bedrock sooner or later can reach −5.27 ℃, i.e. slightly higher than in the previous case (Figure 7, line 1).

According to current understanding, the past six decades have witnessed a steady reduction in glacier mass worldwide, driven by climate change, rising temperatures, and shifts in precipitation patterns. The average rate of mass loss for glaciers in the Russian Arctic ranges from 0.5 to 1 $m \cdot a^{-1}$, though in some cases this figure can be even higher (Hugonnet et al., 2021; Zemp et al., 2009). However, it is expected that the rate of loss will accelerate with further warming. Therefore, within the framework of this study, calculations for the SSP1-2.6 climate scenario were also performed under conditions of gradual glacier degradation at rates of 1, 2, and 3 $m \cdot a^{-1}$, respectively. The temporal evolution of subglacial temperature for these scenarios is shown in curves 3, 4, and 5 of Figure 7. The modeling results indicate that glacier degradation leads to a reduction in its insulating properties, which is relatively self-evident. This, in turn, slows the rate of temperature increase at the bed and will ultimately hinder the formation of a subglacial water body. If such a water body has already formed, glacier degradation would likely also lead to its degradation through gradual freezing.

5 Discussions

The numerical experiments conducted in this study provide valuable insights into the potential formation of subglacial lakes in the Franz Josef Land archipelago, while also highlighting the challenges associated with modeling such phenomena under conditions of limited data availability. The results underscore the significant influence of initial and boundary conditions on the outcomes of glaciological simulations, particularly over varying time scales.

Experiment 1 demonstrated that initial conditions play a critical role in short-term modeling, as evidenced by the rapid formation and subsequent degradation of a subglacial lake within the first 211 a of simulation. The unrealistic assumption of a constant initial temperature distribution led to transient artifacts, such as the bending of temperature profiles and the temporary formation of a lake. However, as the simulation progressed, the system gradually approached equilibrium, and the influence of boundary conditions—such as the geothermal heat flow—became dominant. This experiment emphasizes the importance of accurate initial temperature distributions for reliable short-term predictions, while also illustrating how boundary conditions govern long-term behavior.

In Experiment 2, the use of a more realistic initial temperature distribution, derived from field data, yielded results that were consistent with current climatic conditions. The absence of subglacial lake formation by the year 2100 suggests that, under present-day climate scenarios, the thermal regime of the glacier bed remains below the melting point. However, the steady increase in basal temperatures over time (reaching −5.23 ℃ by 2100) indicates a potential trajectory toward melting in the future, should warming trends persist. This experiment highlights the sensitivity of glacier bed temperatures to GHF and long-term climatic trends.

Experiment 3, which incorporated the IPCC SSP1-2.6 scenario, further explored the impact of climate change on glacier thermal dynamics. Despite the optimistic assumptions of this scenario—limiting global warming to below 2 ℃—the results showed only a marginal increase in basal temperatures (−5.27 ℃ by 2100) compared to Experiment 2. This suggests that even under stringent mitigation policies, the thermal inertia of thick glaciers may delay significant changes in basal conditions over the coming decades. Nevertheless, the long-term implications of sustained warming, combined with geothermal heating, could eventually lead to subglacial melting.

The theoretical estimates presented in Figure 8 provide additional context for understanding the conditions under which subglacial lakes might form. These calculations, though simplified, indicate that basal melting becomes feasible for glaciers exceeding 300 m in thickness, even under moderate geothermal heat flows (60 $mW \cdot m^{-2}$). The variability in surface temperatures (θ_0) further underscores the need for precise field measurements to constrain model inputs. The absence of comprehensive radar or satellite data for the Franz Josef Land archipelago remains a significant limitation, as such tools could validate model predictions and identify existing subglacial water bodies.

Furthermore, our model does not account for potential changes in snow cover dynamics and surface meltwater infiltration, which could significantly influence the subglacial thermal regime. For instance, increased winter precipitation could lead to a thicker snowpack with enhanced insulating properties, reducing winter cooling and potentially resulting in higher basal temperatures than projected. Conversely, a reduction in snow cover would amplify basal freezing. The same situation applies to wind-driven snow redistribution. This is applicable especially for fresh snow, which is, on one hand, mobile,

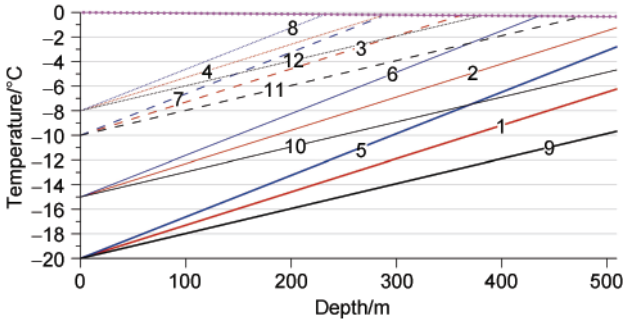

Figure 8 Temperatures on the bottom of the glacier with a condition of stationarity and lack of spreading. 1, θ_0=−20 ℃, Λ_G=60 mW·m^{-2}; 2, θ_0=−15 ℃, Λ_G=60 mW·m^{-2}; 3, θ_0=−10 ℃, Λ_G=60 mW·m^{-2}; 4, θ_0=−8 ℃, Λ_G=60 mW·m^{-2}; 5, θ_0=−20 ℃, Λ_G= 75 mW·m^{-2}; 6, θ_0=−15 ℃, Λ_G=75 mW·m^{-2}; 7, θ_0=−10 ℃, Λ_G=75 mW·m^{-2}; 8, θ_0=−8 ℃, Λ_G=75 mW·m^{-2}; 9, θ_0=−20 ℃, Λ_G=45 mW·m^{-2}; 10, θ_0=−15 ℃, Λ_G=45 mW·m^{-2}; 11, θ_0=−11 ℃, Λ_G= 45 mW·m^{-2}; 12, θ_0=−8 ℃, Λ_G=45 mW·m^{-2}. Magenta line is phase temperatures.

and, on the other hand, a better thermal insulator (because of more air inside). Wind-driven compaction has the opposite impact. It is related to increasing snow density and reducing air volume, which diminishes its thermal isolating properties. Therefore, this process can change local thermal regime of a glacier. Additionally, intensified surface melting and subsequent meltwater penetration to the glacier bed could serve as an efficient heat transfer mechanism, potentially accelerating basal warming and facilitating subglacial lake formation. All of the above factors are important for the upper part of glacier or for thin glaciers. These feedback mechanisms represent important avenues for future research with more complex, multi-physical models.

The simulation results presented above reflect the presumed state of the subglacial environment under the assumption of a fixed glacier geometry. This constitutes the primary shortcoming and limitation of the model. While methods exist to account for ice flow (Fürst et al., 2011; Greve and Blatter, 2009; Pattyn, 2003, 2010), it is important to recognize that these promising models require high-quality input data regarding boundary and initial conditions. This pertains to both the glacier geometry—specifically its thickness and subglacial topography—and the internal temperature distribution. However, it should be noted that the ice thickness map presented in Figure 1 was compiled from airborne radio-echo sounding profiles with an inter-track spacing of 5 km (Khlyupin et al., 2002; Leonov and Popov, 1997). Given that the largest glaciers have linear dimensions of approximately 60 km, their area contains only about 10 flight lines. Furthermore, the region has only one meteorological station and a single borehole with a temperature record covering just the upper 315 m of the 509 m total ice thickness (Henderson, 2002).

Consequently, the data coverage leaves much to be desired. Additionally, the current climatic situation is extremely complex and, generally speaking, unpredictable in the future. This is because the western part of the archipelago is influenced by the warm Gulf Stream current. This influence is clearly visible in the spatial distribution of ice thickness across the archipelago (Figure 1). According to available oceanographic data and current understanding, the Gulf Stream is expected to weaken; however, the consequences of this weakening for future regional climate changes are difficult to predict (Ditlevsen and Ditlevsen, 2023; Palter, 2015). It is also important to note that this current influences not only heat transport but also precipitation patterns.

Thus, while a precise assessment of the total glacier mass balance may not be feasible, it is evident that the archipelago's glaciers will degrade due to warming. The primary driver of this degradation will likely be accelerated ice flow resulting from the overall increase in ice temperature and the consequent reduction in ice viscosity.

6 Conclusions

This study provides important insights into the thermal dynamics of Arctic glaciers through numerical modeling experiments. Its innovations are that these are the first such investigations to the Franz Josef Land archipelago and the quantification of regional thresholds. The research demonstrates a clear temporal influence in controlling factors: while initial conditions predominantly influence short-term (decadal-scale) model outcomes, boundary conditions including GHF and climatic trends become the dominant drivers in long-term simulations. Of particular significance are the theoretical indications that subglacial water bodies could potentially form beneath ice masses exceeding 300 m in thickness in the Franz Josef Land archipelago under current climatic conditions. However, it is also necessary to note that, given the spatial heterogeneity across the archipelago, the demonstrated quantitative results primarily apply to areas with characteristics similar to those of the Windy Dome.

The modeling results reveal that even under the optimistic SSP1-2.6 climate scenario, which projects limited warming, basal temperatures show a persistent upward trend that could eventually reach the pressure melting point. This delayed response highlights the thermal inertia characteristic of thick Arctic ice masses. However, the study emphasizes that these projections remain constrained by significant data limitations, particularly the lack of comprehensive in situ temperature measurements and high-resolution subsurface imaging.

These findings underscore the urgent need for enhanced observational capabilities through expanded field instrumentation and advanced remote sensing technologies. Such improvements would substantially increase the

reliability of predictive models for Arctic ice mass evolution and their potential contributions to global sea-level rise. The study concludes that while current models provide valuable theoretical understanding, their predictive power remains limited without better empirical constraints on both initial conditions and boundary parameters.

Acknowledgments We thank two anonymous reviewers and Associate Editor Chen Zhao for their numerous corrections and suggestions for improving the English, which enabled us to significantly enhance the manuscript. This research was partly supported by the Shanghai Science and Technology Innovation Action Plan (Grant no. 23230712200).

References

Boronina A, Popov S, Qiao G. 2024. On the factors and the degree of their effect on subglacial melt and changes in the state of Antarctic subglacial lakes. Arct Antarct Alp Res, 56(1): 2406622, doi:10.1080/15230430.2024.2406622.

Dickinson R E, Henderson-Sellers A, Kennedy P J, et al. 1986. Biosphere-atmosphere transfer scheme (BATS) for the NCAR community climate model (NCAR/TN-275+STR). Boulder: National Center for Atmospheric Research.

Ditlevsen P, Ditlevsen S. 2023. Warning of a forthcoming collapse of the Atlantic meridional overturning circulation. Nat Commun, 14(1): 4254, doi:10.1038/s41467-023-39810-w.

Eckel O, Thams C. 1939. Investigations on conditions of density, temperature, and radiation of the Davos snow cover. Wilmette: Snow, Ice and Permafrost Research Establishment Translation No.14: 245-304.

Farnsworth W R, Allaart L, Ingólfsson Ó, et al. 2020. Holocene glacial history of Svalbard: status, perspectives and challenges. Earth Sci Rev, 208: 103249, doi:10.1016/j.earscirev.2020.103249.

Fürst J J, Rybak O, Goelzer H, et al. 2011. Improved convergence and stability properties in a three-dimensional higher-order ice sheet model. Geosci Model Dev, 4(4): 1133-1149, doi:10.5194/gmd-4-1133-2011.

Gelfan A N, Moreido V M. 2014. Dynamic-stochastic modeling of snow cover formation on the European territory of Russia. Lëd I Sneg, 54(2): 44-52, doi:10.15356/2076-6734-2014-2-44-52 (in Russian with English abstract).

Glen J W. 1953. Rate of flow of polycrystalline ice. Nature, 172(4381): 721-722, doi:10.1038/172721a0.

Gramberg I S, Shkola I V, Bro E G, et al. 1985. Parametric wells on the islands of the Barents and Kara Seas. Soviet Geol, 1: 95-98 (in Russian).

Greve R, Blatter H. 2009. Dynamics of ice sheets and glaciers. Dordrecht, New York: Springer.

Groswald M G, Krenke A N, Vinogradov O N, et al. 1973. Franz Josef Land glaciation. Moscow: Nauka (in Russian).

Hedstrom N, Pomeroy J W. 1998. Measurements and modelling of snow interception in the boreal forest. Hydrol Process, 12: 1611-1625, doi:10.1002/(SICI)1099-1085(199808/09)12:10/11<1611::AID-HYP684>3.0.CO;2-4.

Henderson K A. 2002. An ice core paleoclimate study of Windy Dome, Franz Josef Land (Russia): development of a recent climate history for the Barents Sea. Ph.D. thesis, Columbus: Ohio State University.

Hugonnet R, McNabb R, Berthier E, et al. 2021. Accelerated global glacier mass loss in the early twenty-first century. Nature, 592(7856): 726-731, doi:10.1038/s41586-021-03436-z.

Kapitsa A P, Ridley J K, Robin G de Q, et al. 1996. A large deep freshwater lake beneath the ice of central East Antarctica. Nature, 381(6584): 684-686, doi:10.1038/381684a0.

Karyakin Yu V, Kashkarov N N. 2011. Statistical model of the relief of Franz Josef Land. Proceed Voronezh State Univ Geol Ser, 1: 241-244 (in Russian).

Kastrov V G. 1956. Solar radiation in the troposphere in the case of absolutely clean air. Trudy CAO, 16: 26-30 (in Russian).

Khlyupin N I, Leonov V O, Mandrikov V S, et al. 2002. Regional integrated aerogeophysical studies of the PMGE in the Arctic region. Razvedka I Okhrana Nedr, 9: 55-58 (in Russian).

Khutorskoy M D, Akhmedzyanov V R, Ermakov A V, et al. 2013. Geothermics of the Arctic seas. Moscow: GEOS (in Russian).

Kominami Y, Endo Y, Niwano S, et al. 1998. Viscous compression model for estimating the depth of new snow. Ann Glaciol, 26: 77-82, doi:10.3189/1998aog26-1-77-82.

Krenke A N, Voronina L S. 1964. General meteorological observations. Glaciological research materials//Franz Josef Land: meteorology. Leningrad: Gidrometeoizdat.

Leonov V O, Popov S V. 1997. Bedrock of the Franz Josef Land by data of the radio-echo and magnetic sounding. Data Glaciol Stud, 82: 208-212 (in Russian).

Livingstone S J, Li Y, Rutishauser A, et al. 2022. Subglacial lakes and their changing role in a warming climate. Nat Rev Earth Environ, 3(2): 106-124, doi:10.1038/s43017-021-00246-9.

Lubinski D J, Forman S L, Miller G H. 1999. Holocene glacier and climate fluctuations on Franz Josef Land, Arctic Russia, 80°N. Quat Sci Rev, 18(1): 85-108, doi:10.1016/S0277-3791(97)00105-4.

Marshall H P, Conway H, Rasmussen L A. 1999. Snow densification during rain. Cold Reg Sci Technol, 30(1-3): 35-41, doi:10.1016/S0165-232X(99)00011-7.

Martos Y M, Catalán M, Jordan T A, et al. 2017. Heat flux distribution of Antarctica unveiled. Geophys Res Lett, 44: 11417-11426, doi:10.1002/2017gl075609.

Motovilov Y G, Zhidkov V A. 1986. Modelling of snow cover properties in periods of its formation and melting. Data Glaciol Stud, 56: 50-56 (in Russian).

Osokin N I, Sosnovsky A V. 2015. Impact of dynamics of air temperature and snow cover thickness on the ground freezing. Kriosfera Zemli, 19(1): 99-105 (in Russian with English abstract).

Osokin N I, Samoilov R S, Sosnovskii A V, et al. 1999. On estimation the influence of snow cover characteristics variability on soils freezing. Kriosfera Zemli, 3(1): 3-10 (in Russian).

Palter J B. 2015. The role of the gulf stream in European climate. Annu Rev Mar Sci, 7: 113-137, doi:10.1146/annurev-marine-010814-015656.

Paterson W S B. 1994. Physics of glaciers. Oxford: Butterworth-Heinemann.

Pattyn F. 2003. A new three-dimensional higher-order thermomechanical ice sheet model: basic sensitivity, ice stream development, and ice flow across subglacial lakes. J Geophys Res Solid Earth, 108(B8): 2002JB002329, doi:10.1029/2002JB002329.

Pattyn F. 2010. Antarctic subglacial conditions inferred from a hybrid ice

sheet/ice stream model. Earth Planet Sci Lett, 295(3/4): 451-461, doi:10.1016/j.epsl.2010.04.025.

Popov S V. 2022. Ice cover, subglacial landscape, and estimation of bottom melting of Mac. Robertson, Princess Elizabeth, Wilhelm II, and western Queen Mary Lands, East Antarctica. Remote Sens, 14(1): 241, doi:10.3390/rs14010241.

Popov S V. 2023. Solution of the one-dimensional Stefan problem with two transitions for modelling of the water freezing in a glacial crevasse. Lëd I Sneg, 63(1): 130-140, doi:10.31857/s2076673423010131 (in Russian with English abstract).

Popov S V, Boronina A S, Lebedeva L S. 2023. The main factors in the formation of subaerial taliks on the example of the Shestakovka River basin (Central Yakutia), using a one-dimensional mathematical model. Lëd I Sneg, 63(4): 597-611, doi: 10.31857/S2076673423040130 (in Russian with English abstract).

Popov S V, Boronina A S, Ekaykin A A, et al. 2024a. Remote sensing and mathematical modelling of Lake Vostok, East Antarctica: past, present and future research. Arctic Antarct Res, 70(4): 460-476, doi:10.30758/0555-2648-2024-70-4-460-476.

Popov S V, Boronina A S, Nemchinova A V, et al. 2024b. Formation of subaerial taliks in Larsemann Hills, Princess Elizabeth Land, East Antarctica. Polar Sci, 40: 101070, doi:10.1016/j.polar.2024.101070.

Prohaska F, Thams C. 1940. New research on the radiational properties of the snow cover. Helvetica Physica Acta, 13: 21-44 (in German).

Ridley J K, Cudlip W, Laxon S W. 1993. Identification of subglacial lakes using ERS-1 radar altimeter. J Glaciol, 39(133): 625-634, doi:10.3189/s002214300001652x.

Robin G de Q. 1955. Ice movement and temperature distribution in glaciers and ice sheets. J Glaciol, 2(18): 523-532, doi:10.3189/002214355793702028.

Samarskii A A, Moiseyenko B D. 1965. An economic continuous calculation scheme for the Stefan multidimensional problem. USSR Comput Math Math Phys, 5(5): 43-58, doi:10.1016/0041-5553(65)90004-2.

Samarskii A A, Vabishchevich P N. 2003. Computational heat transfer. Moscow: Editorial URSS Publisher (in Russian).

Samarskii A A, Vabishchevich P N. 2009. Computational heat and mass transfer. Moscow: Librokom (in Russian).

Schroeder D M, Bingham R G, Blankenship D D, et al. 2020. Five decades of radioglaciology. Ann Glaciol, 61(81): 1-13, doi:10.1017/aog.2020.11.

Shipilov E V, Shkarubo S I, Matishov G G, et al. 2018. New data on Franz Josef Land tectonic (archipelago and shelf, northern segment of the continental margin of the Barent Sea). Dokl Earth Sci, 483: 1388-1393, doi: 10.1134/S1028334X18110065.

Sivkov S I. 1968. Methods for calculating the characteristics of solar radiation. Leningrad: Gidrometeoizdat (in Russian).

Sosnovsky A V. 1984. Calculation of the optimal thickness of the water-ice mixture layer when freezing ice over large areas. Data Glaciol Stud, 50: 223-231 (in Russian).

Sosnovsky A V. 2006. Mathematical modelling of the influence of snow cover thickness on degradation of permafrost at climate warming. Kriosfera Zemli, 10(3): 83-88 (in Russian).

Sukhanova A, Bantsev D, Popov S, et al. 2023. The current state of Lake Dålk (Larsemann Hills, East Antarctica). Polar Sci, 38: 101006, doi:10.1016/j.polar.2023.101006.

Surkova G V, Vasil'chuk Y K. 2022. Comparison of simulated and reconstructed paleotemperatures during the last glacial maximum in Northern Eurasia. Vestnik Moskovskogo Universiteta, 6: 40-48 (in Russian with English abstract).

Vasil'chuk Y K, Surkova G V. 2020. Verification of the relationship between the isotopic composition of ice wedges and cold-season temperature over the recent 80 years in the northern permafrost zone of Russia. Russ Meteorol Hydrol, 45(11): 791-796, doi:10.3103/s1068373920110060.

Vasilyev V I, Vasilyeva M V, Stepanov S P, et al. 2021. Numerical solution of the two-phase Stefan problem in the enthalpy formulation with smoothing the coefficients. Her Bauman Mosc State Tech Univ Ser Nat Sci, 97: 4-23, doi:10.18698/1812-3368-2021-4-4-23.

Vinogradov Y B. 1988. Mathematical modelling of runoff formation processes. Leningrad: Gidrometizdat.

Virkkunen K, Moore J C, Isaksson E, et al. 2007. Warm summers and ion concentrations in snow: comparison of present day with Medieval Warm Epoch from snow pits and an ice core from Lomonosovfonna, Svalbard. J Glaciol, 53(183): 623-634, doi:10.3189/002214307784409388.

Zemp M, Hoelzle M, Haeberli W. 2009. Six decades of glacier mass-balance observations: a review of the worldwide monitoring network. Ann Glaciol, 50(50): 101-111, doi:10.3189/172756409787769591.

Zotikov I A. 1963. Bottom melting in the central zone of the ice shield on the Antarctic continent and its influence upon the present balance of the ice mass. Int Assoc Sci Hydrol Bull, 8(1): 36-44, doi:10.1080/02626666309493295.